Journal of Physiology (1993), **469**, *pp.* 341–363
With 8 figures
Printed in Great Britain

AN IONIC CURRENT MODEL FOR NEURONS IN THE RAT MEDIAL NUCLEUS TRACTUS SOLITARII RECEIVING SENSORY AFFERENT INPUT

BY J. H. SCHILD*, S. KHUSHALANI*, J. W. CLARK*, M. C. ANDRESEN†, D. L. KUNZE‡ AND M. YANG†

*From the *Department of Electrical and Computer Engineering, Rice University, Houston, TX 77251, the †Department of Physiology and Biophysics, University of Texas Medical Branch, Galveston, TX 77550 and the ‡Department of Molecular Physiology and Biophysics, Baylor College of Medicine, Houston, TX 77030, USA*

(*Received 16 September 1991*)

SUMMARY

1. Neurons from a horizontal slice of adult rat brainstem were examined using intracellular recording techniques. Investigations were restricted to a region within the nucleus tractus solitarii, medial to the solitary tract and centred on the obex (mNTS). Previous work has shown this restricted area of the NTS to contain the greatest concentration of aortic afferent baroreceptor terminal fields. Electrical stimulation of the tract elicited short-latency excitatory postsynaptic potentials in all neurons.

2. mNTS neurons were spontaneously active with firing frequencies ranging between 1 and 10 Hz, at resting potentials of −65 to −45 mV. These neurons did not exhibit spontaneous bursting activity.

3. Depolarizing current injection immediately evoked a finite, high-frequency spike discharge which rapidly declined to a lower steady-state level (i.e. spike frequency adaptation, SFA). Increasing depolarizations produced a marked increase in the peak instantaneous frequency but a much smaller increase in the steady-state firing level.

4. Conditioning with a hyperpolarizing prepulse resulted in a prolonged delay of up to 600 ms before the first action potential (i.e. delayed excitation, DE) with an attendant decrease in peak discharge rates. DE was modulated by both the magnitude and duration of the prestimulus hyperpolarization, as well as the magnitude of the depolarizing stimulus. Tetrodotoxin (TTX) eliminated spike discharge but had little effect on the ramp-like membrane depolarization characteristic of DE.

5. We have developed a mathematical model for mNTS neurons to facilitate our understanding of the interplay between the underlying ionic currents. It consists of a comprehensive membrane model of the Hodgkin–Huxley type coupled with a fluid compartment model describing cytoplasmic $[Ca^{2+}]_i$ homeostasis.

† Present address: Department of Physiology, Oregon Health Sciences University, Portland, OR 97201, USA.

MS 9740

6. The model suggests that (a) SFA is caused by an increase in $[Ca^{2+}]_i$ which activates the outward K^+ current, $I_{K,Ca}$, and (b) DE results from the competitive interaction between the injected depolarizing current and the hyperpolarization-activated transient outward K^+ currents, I_A and I_D.

7. We conclude that our ionic current model is capable of providing biophysical explanations for a number of phenomena associated with brainstem neurons, either during spontaneous activity or in response to patterned injections of current. This model is a potentially useful adjunct for on-going research into the central mechanisms involved in the regulation of both blood pressure and ventilation.

INTRODUCTION

Primary afferent fibres from peripheral chemoreceptors, baroreceptors and pulmonary mechanoreceptors enter the brainstem and synapse in the nucleus of the tractus solitarius (NTS) (Loewy, 1990). Portions of NTS are known to act as an important premotor integrating centre for cardiorespiratory reflexes in many species. Within the rat NTS, the integrity of the dorsomedial region is essential to baroreflex control of arterial blood pressure (Reis, 1984). Considerable overlap of sensory afferents of different modalities has been suggested (Loewy, 1990). Synaptic drive, intrinsic membrane properties and modulatory inputs must collectively determine the pattern of activity displayed by NTS neurons.

Using transganglionic transport of horseradish peroxidase (Kunze, Yang & Andresen, 1990) or the fluorescent, lipophilic dye, DiA (Mendelowitz, Yang, Andresen & Kunze, 1992), we have found the majority of aortic nerve terminals to lie in a relatively restricted region of dorsomedial NTS near the obex and generally medial to the solitary tract (mNTS). In the rat, the aortic nerve contains only arterial baroreceptor afferent axons (Sapru & Krieger, 1977) so that these terminal fields of the aortic nerve represent baroreceptor inputs to mNTS. In the present study, an *in vitro* brainstem slice preparation was used to examine the membrane properties of rat NTS neurons from this medial region. A variety of ionic currents have been identified for neurons isolated from this area of mNTS (Kunze, 1987) and from slice preparations of other NTS regions (Champagnat, Jacquin & Richter, 1986; Dekin & Getting, 1987). We have developed an ionic current model for the mNTS neuron to provide a quantitative integrated description of the ionic macrocurrents present in the soma of the cell and their interaction in the genesis of patterned electrical activity. The model describes the electrical behaviour of the mNTS neuron in response to different sequences of depolarizing and hyperpolarizing current pulses, and provides a biophysical explanation for the various phenomena observed in these tests.

METHODS

Experimental procedure

Tissue preparation

Methods for preparing the horizontal slices of the medulla were identical to those previously described (Andresen & Yang, 1990). Briefly, male rats (Sprague–Dawley, 150–250 g) were anesthetized with ether, and quickly killed by severing the carotid arteries and jugular veins in the neck. The hindbrain was rapidly removed and placed in cold perfusate (0–2 °C) gassed with 95%

O_2–5% CO_2. The brain was trimmed rostrally and caudally so that the remnant piece centred on the obex. The remaining tissue was sectioned longitudinally into 400 μm slices at an angle which provided the maximum length of the solitary tract to be preserved along with the NTS. Tissue slices were then placed in a perfusion chamber (34–37 °C), and partially submerged for interfacial superfusion of the lower surface. The perfusate was continuously bubbled with a gas mixture of 95% O_2–5% CO_2, and bath pH was maintained at 7·4. The composition of the perfusate was (mM): 120 NaCl, 4·8 KCl, 1·2 KH_2PO_4, 1·2 $MgSO_4$, 25 $NaHCO_3$, 5·5 dextrose, 2 $CaCl_2$.

Recording

Glass microelectrodes (4 M potassium asparate; 80–120 MΩ), connected to an Axoclamp 2A amplifier (Axon Instruments), were used to measure intracellular potential. The microelectrode was positioned (under direct observation with a stereo-microscope) into restricted areas of the NTS. Specifically, the area of recording was limited to a maximum of 400 μm rostral or caudal to the obex, and always medial to the solitary tract. This region of the NTS is known to receive the highest density of aortic baroreceptor afferent projection in the rat (Ciriello, 1983; Kunze *et al.* 1990; Mendelowitz *et al.* 1992). Criteria for a successful neuron impalement included a minimum of 15 min recording with a stable membrane potential of greater than −45 mV, an action potential amplitude greater than 60 mV, and a cell input resistance greater than 50 MΩ. A concentric bipolar electrode was placed on the solitary tract 1–3 mm from the NTS recording site, and 100 μs pulses were delivered to the tract to elicit synaptic potentials in the NTS neurons. All neurons included in this study showed short-latency (< 3 ms), excitatory postsynaptic potentials upon tract stimulation. Sequentially applied hyperpolarizing and depolarizing pulses of current could be delivered via the intracellular microelectrode using the Axoclamp 2A amplifier in the bridge mode. Typical resting membrane potentials and input resistance in mNTS neurons studied were $-51{\cdot}1 \pm 0{\cdot}8$ mV and $63{\cdot}3 \pm 2{\cdot}7$ MΩ ($n = 75$), respectively (mean ± S.E.M.). Responses were recorded on a VHS video cassette recorder via an encoding unit (PCM 4, Medical Systems) in 2-channel mode (44 kHz sampling rate) for playback and analysis after the experiment.

Some experiments were conducted with microelectrodes filled with a solution of 2% Lucifer Yellow dye (Sigma, USA) in 1 M lithium chloride. After completing electrophysiological studies, dye was iontophoretically injected into the cells for 15–60 min followed by overnight fixation in 4% paraformaldehyde in 0·1 M sodium phosphate buffer at pH 7·4. Sections (40–50 μm) were made of the original 400 μm slice (Vibrotome) and the Lucifer Yellow dye visualized with anti-Lucifer Yellow antibody (Molecular Probes, Eugene, OR, USA).

Model formulation

Our model of the mNTS neuron consists of two components (Fig. 1*A* and *B*), a Hodgkin–Huxley (HH)-type parallel conductance membrane model (Hodgkin & Huxley, 1952) and a lumped fluid compartment model. The HH equivalent electrical circuit (Fig. 1*A*) comprises a membrane capacitance, C_m, shunted by time- and voltage-dependent ion-selective channels, in addition to pump, exchanger and other background currents. The lumped fluid compartment model (Fig. 1*B*) comprises two well-stirred compartments containing different concentrations of Na^+, K^+ and Ca^{2+}. The first compartment describes the intracellular space and includes effective binding sites for Ca^{2+} such as those on calmodulin. The second compartment represents a large extracellular volume where ionic concentrations ($[Ca^{2+}]_o$, $[Na^+]_o$, $[K^+]_o$) are assumed to be constant.

Membrane model

Under space clamp conditions, the differential equation describing the time-dependent changes in the membrane potential (V) is:

$$\dot{V} = \frac{-(I_{Na}+I_{Ca,L}+I_K+I_{K,Ca}+I_A+I_D+I_R+I_B+I_{NaK}+I_{NaCa}+I_{CaP}-I_{STIM})}{C_m} \quad (1)$$

where C_m is the whole-cell membrane capacitance. The fast Na^+ current (I_{Na}), the high-threshold, long-lasting Ca^{2+} current ($I_{Ca,L}$), the delayed rectifier current (I_K), the transient outward current (I_A), and the delay current (I_D) have been modelled as voltage- and time-dependent ionic currents. A Ca^{2+}-activated K^+ current ($I_{K,Ca}$) has been modelled as both a voltage- and Ca^{2+}-dependent current, as is the Na^+–Ca^{2+} exchanger current (I_{NaCa}). I_{NaCa} plays a very important role in cytosolic

calcium balance since calcium concentration in the bathing medium is held constant, while intracellular calcium ($[Ca^{2+}]_i$) varies with membrane voltage and time under the influence of several factors affecting Ca^{2+} -balance in this cell (see the material balance for $[Ca^{2+}]_i$ given in eqn. (4)). The concentrations of Na^+ and K^+ in the intra- and extracellular media are also assumed to be constant.

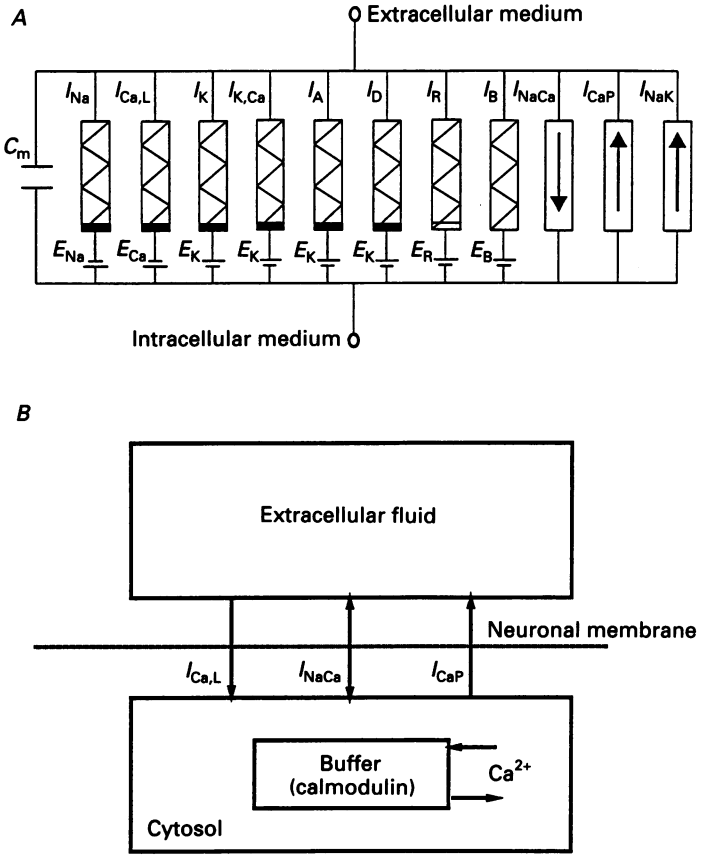

Fig. 1. Equivalent circuit of a medial NTS neuron. Figure 1*A* shows the membrane model of the cell. The membrane capacitance C_m is shunted by time- and voltage-dependent sodium, calcium, and potassium channel-mediated currents (I_{Na}, $I_{Ca,L}$, I_K), a Ca^{2+}-activated potassium current ($I_{K,Ca}$), a transient outward current (I_A), a delay current (I_D), an inward rectifier current (I_R), a linear leakage current (I_B), and electrogenic transporter-mediated currents (Na^+–Ca^{2+} exchanger, Na^+–K^+ pump, Ca^{2+} pump). E_{Na}, E_K and E_{Ca} are the equilibrium potentials for sodium, potassium and calcium, respectively. Figure 1*B* shows the lumped fluid compartmental model. This model consists of two separate well-stirred fluid compartments containing Na^+, K^+ and Ca^{2+} in different concentrations. The two compartments are: (a) an intracellular fluid space that contains protein binding sites for Ca^{2+} on a calmodulin-type buffer, and (b) a large extracellular volume where all ionic concentrations ($[Ca^{2+}]_o$, $[Na^+]_o$, $[K^+]_o$) are assumed to be constant.

Thus for specified values of $[Na^+]_i$ and $[K]_o$, the Na^+–K^+ pump current (I_{NaK}) behaves as a purely voltage-dependent outward current, while the Ca^{2+} pump current (I_{CaP}) depends solely on $[Ca^{2+}]_i$ which changes during electrical activity. The non-linear inward rectifier current (I_R) is solely voltage-dependent. I_B is a linear background current and I_{STIM} corresponds to the injected current.

The HH-type gating variables in these equations are solutions of first-order differential equations of the general form

$$\dot{z} = \frac{z_\infty - z}{\tau_z}, \tag{2}$$

where z_∞ refers to steady-state conditions, τ_z the solution time constant and where $z = m, h, d_L, f_L, n, p, q_1, q_2, x, y$ or c depending upon the particular channel current (see below). This nomenclature conforms to convention as much as possible. For each ion channel current, appropriate equation sets consistent with eqn. (2) were either: (a) formulated according to numerical fits to whole-cell voltage-clamp data recorded in our laboratory (see below) or (b) adopted from the literature, with necessary adjustments for consistency with our experimental conditions (e.g. rate constants were adjusted by temperature scaling (Q_{10}) factors to 37 °C).

TABLE 1. Inward currents

I_{Na}: sodium current

$$I_{Na} = \bar{g}_{Na} m^3 h (V - E_{Na})$$

$$\dot{m} = \frac{m_\infty - m}{\tau_m} \qquad \dot{h} = \frac{h_\infty - h}{\tau_h}$$

$$\alpha_m = \frac{0{\cdot}36(V + 35{\cdot}0)}{1 - \exp(-(V + 35{\cdot}0)/3{\cdot}0)}$$

$$\tau_h = 1{\cdot}15 \exp(-(0{\cdot}055)^2 (V + 29{\cdot}62)^2) + 0{\cdot}15$$

$$\beta_m = \frac{-0{\cdot}4(V + 53{\cdot}0)}{1 - \exp((V + 53{\cdot}0)/20{\cdot}0)}$$

$$\tau_m = \frac{2{\cdot}0}{3{\cdot}488(\alpha_m + \beta_m)} + 0{\cdot}05$$

$$m_\infty = \frac{\alpha_m}{\alpha_m + \beta_m} \qquad h_\infty = \frac{1{\cdot}0}{1{\cdot}0 + \exp((V + 29{\cdot}62)/5{\cdot}035)}$$

$I_{Ca,L}$: long-lasting calcium current

$$I_{Ca,L} = \bar{g}_{Ca,L} d_L^2 f_L (V - E_{Ca,L})$$

$$\dot{d}_L = \frac{d_{L_\infty} - d_L}{\tau_{d_L}} \qquad \dot{f}_L = \frac{f_{L_\infty} - f_L}{\tau_{f_L}}$$

$$d_{L_\infty} = \frac{1{\cdot}0}{1{\cdot}0 + \exp(-(V + 2{\cdot}8)/9{\cdot}85)} \qquad f_{L_\infty} = \frac{1{\cdot}0}{1{\cdot}0 + \exp((V + 14{\cdot}61)/4{\cdot}5)}$$

$$\tau_{d_L} = (0{\cdot}3426 \exp(0{\cdot}0925V) + 1{\cdot}8818 \exp(-0{\cdot}00732V))^{-1} + 0{\cdot}1$$

$$\tau_{f_L} = (0{\cdot}2419 \exp(0{\cdot}145V) + 0{\cdot}0434 \exp(-0{\cdot}02013V))^{-1} + 17{\cdot}0$$

Inward currents

Fast sodium current (I_{Na}). Application of a perfusion medium solution containing 30 μM TTX to the brainstem slice preparation eliminated fast spike discharges. Therefore, we have included a fast, voltage- and time-dependent, TTX-sensitive I_{Na} current in our model. The general form of equations describing the non-linear dynamics of the activation (m^3) and inactivation (h) gating variables associated with the Na^+ channel (Table 1) were modified from the modelling work of Yamada, Koch & Adams (YKA) for a bullfrog sympathetic ganglion cell (Yamada *et al.* 1989).

Long-lasting calcium current ($I_{Ca,L}$). $I_{Ca,L}$ has been observed in all the known NTS cell types (Dekin & Getting, 1987; Kunze, 1987; Haddad & Getting, 1989). It activates rapidly but has slow inactivation characteristics, contributing significantly during spike repolarization. The general

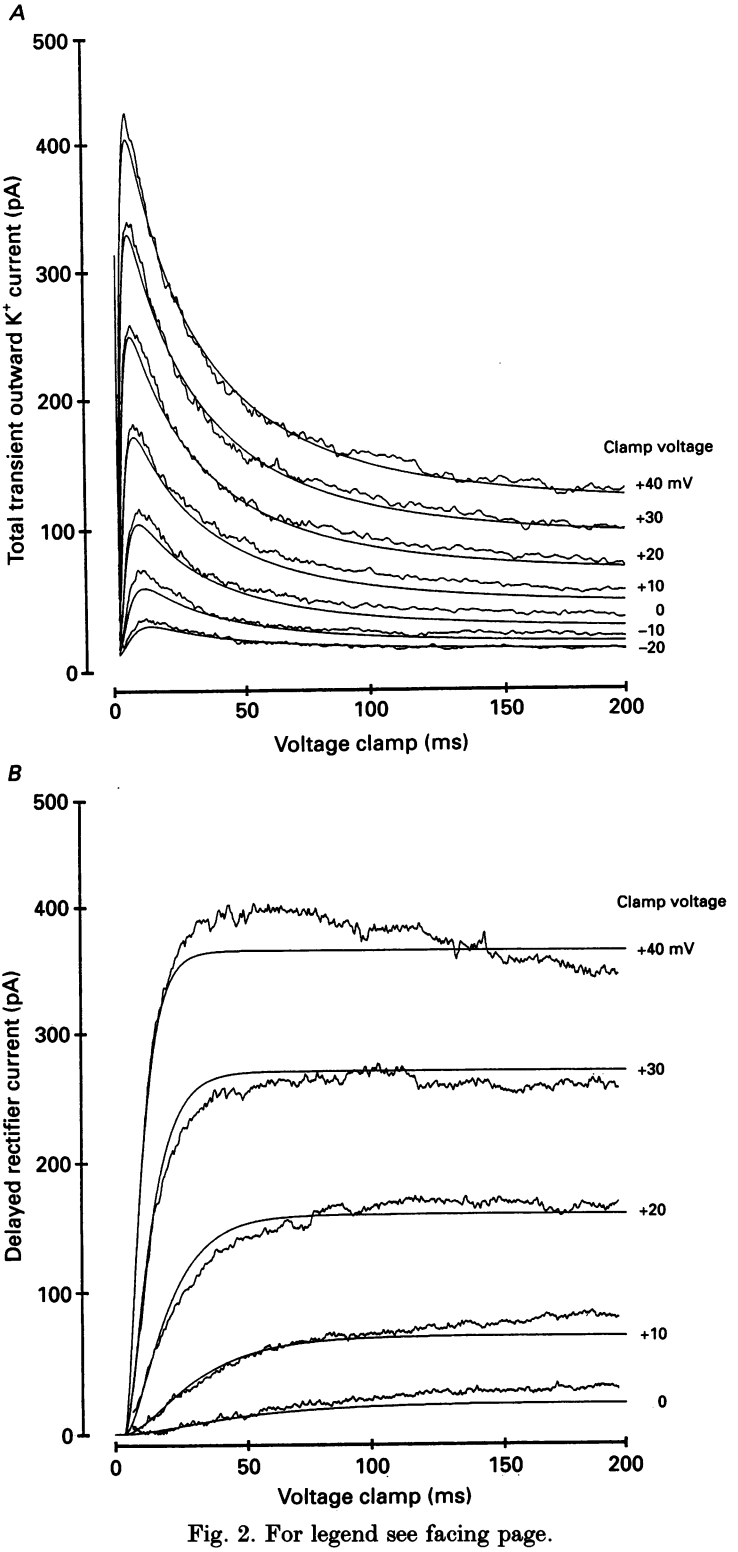

Fig. 2. For legend see facing page.

form of equations describing the activation (d_L^2) and inactivation (f_L) variables of this long-lasting Ca^{2+} channel (Table 1) were adopted from Belluzzi & Sacchi (1989, 1991) where $I_{Ca,L}$ was characterized in adult rat sympathetic neurons.

Outward currents

Transient outward K^+ currents (I_A and I_D). The transient outward K^+ currents I_A and I_D are generally believed to be involved in the encoding of graded depolarizations into spike train information. Although both currents have been observed in many mammalian neurons (Rogawski, 1985; Zbciz & Weight, 1985; Champagnat *et al.* 1986; Numann, Wadman & Wong, 1987; Dekin & Getting, 1987; Storm, 1988; Kasai, Kameyama & Yamaguchi, 1986; Greene, Haas & Reiner, 1990; Thorn, Wang & Lemos, 1991) no consistent formulations or even agreement on current dynamics were available in the literature. Therefore, the expressions used to characterize these currents were based upon numerical fits to typical whole-cell voltage-clamp recordings performed in our laboratory on enzymatically dispersed mNTS neurons (guinea-pig; J. Moak & D. Kunze, unpublished observations).

In response to step increases in clamp voltage, the total transient outward K^+ current in these isolated mNTS neurons exhibits an initial transient onset and decay followed by a plateau phase with extremely slow inactivation characteristics. Activation time constants for I_A and I_D possessed a slight voltage dependence, while current decay proved to be voltage independent. Nominal parameter values associated with mathematical descriptions of these general characteristics were refined using a Marquardt (Marquardt, 1963) non-linear parameter estimation algorithm which provided a good least-squares fit to the whole-cell voltage-clamp data from the enzymatically dispersed mNTS neurons. The quality of these fits is demonstrated in Fig. 2*A*, where the recorded transient outward K^+ current was approximated as the sum of the model-generated I_A and I_D currents. The equation sets from these fits formed basis functions which were further refined using the Marquardt algorithm in order to provide a more exact match to the experimental data from the brainstem slice preparation (see Table 2).

Delayed rectifier current (I_K). Characterization of the transient outward K^+ currents in guinea-pig mNTS neurons also afforded us the opportunity to investigate the I_K current in this species. These experiments demonstrated that I_K responds as a classical, TEA-sensitive delayed rectifier current and in this model serves its usual function of accelerating spike repolarization. The stereotypical kinetics of this current can be observed in the whole-cell voltage-clamp recording of Fig. 2*B* along with the results of numerical fits to these data (see Table 2).

Calcium-activated K^+ current ($I_{K,Ca}$). There is considerable evidence supporting the presence of a Ca^{2+}-activated K^+ current in NTS neurons (Champagnat *et al.* 1986; Dekin & Getting, 1987; Dekin & Haddad, 1990). $I_{K,Ca}$ is believed to play a pivotal role in SFA which has been observed to varying degrees in mNTS neurons. In our model, expressions for $I_{K,Ca}$ have been adapted from the modelling work of YKA (Yamada *et al.* 1989) where the rate of channel opening is considered both voltage and $[Ca^{2+}]_i$ dependent, while the rate of channel closing is solely voltage dependent (Table 2).

Fig. 2. Least-squares fits (smooth traces) to whole-cell voltage-clamp records of the total transient outward K^+ current (Fig. 2*A*) and delayed rectifier current I_K (Fig. 2*B*) from enzymatically dispersed mNTS neurons from guinea-pig (at 23 °C). The mNTS neurons were prepared (Mendelowitz *et al.* 1992) in a manner described elsewhere. Voltage-clamp recordings were performed using conventional activation protocols from a holding potential of −80 mV (J. Moak & D. Kunze, unpublished observations; bathing solution (mM): 137 NaCl, 5·4 KCl, 1 $MgCl_2$, 10 glucose, 10 Hepes and 0·01 TTX and pipette solution (mM): 140 potassium aspartate, 3 $MgCl_2$, 5 EGTA and 10 Hepes. Both sets of data records are the result of subtractive measurements of successive clamp protocols before and after bath application of selective pharmacological channel blockers. For the transient outward K^+ current, 4-aminopyridine (5 mM) was used to ensure accurate recording of I_A and I_D and thereby minimize the possibility of the delayed rectifier contaminating the 'plateau phase' of the data records. I_K was recorded in a similar manner but the blocking agent was TEA (30 mM). All experimental records were smoothed using a 7-point median filter.

TABLE 2. Outward currents

I_A: early transient outward current

$$I_A = \bar{g}_A p^3(0{\cdot}5q_1 + 0{\cdot}5q_2)(V - E_K)$$

$$\dot{p} = \frac{p_\infty - p}{\tau_p}$$

$$\tau_p = 5{\cdot}5\exp(-(0{\cdot}022)^2(V+65{\cdot}0)^2) + 1{\cdot}0$$

$$p_\infty = \frac{1{\cdot}0}{1+\exp([V+51{\cdot}83144]/-13{\cdot}80238)}$$

$$\dot{q}_1 = \frac{q_{1_\infty} - q_1}{\tau_{q_1}}$$

$$\tau_{q_1} = 70{\cdot}0$$

$$q_{1_\infty} = \frac{1{\cdot}0}{1{\cdot}0+\exp([V+73{\cdot}0]/4{\cdot}66667)}$$

$$\dot{q}_2 = \frac{q_{2_\infty} - q_2}{\tau_{q_2}}$$

$$\tau_{q_2} = 550{\cdot}0$$

$$q_{2_\infty} = \frac{1{\cdot}0}{1{\cdot}0+\exp([V+73{\cdot}0]/4{\cdot}66667)}$$

I_D: slowly inactivating delay current

$$I_D = \bar{g}_D x^3 y(V - E_K)$$

$$\dot{x} = \frac{x_\infty - x}{\tau_x}$$

$$\tau_x = 5{\cdot}5\exp(-(0{\cdot}022)^2(V+65{\cdot}0)^2) + 1{\cdot}0$$

$$x_\infty = \frac{1{\cdot}0}{1+\exp([V+31{\cdot}83144]/-13{\cdot}13572)}$$

$$\dot{y} = \frac{y_\infty - y}{\tau_y}$$

$$\tau_y = 6500{\cdot}0$$

$$y_\infty = \frac{1{\cdot}0}{1+\exp([V+63{\cdot}0]/4{\cdot}66667)}$$

I_K: delayed rectifier

$$I_K = \bar{g}_K n^2(V - E_K)$$

$$\dot{n} = \frac{n_\infty - n}{\tau_n}$$

$$\tau_n = 60{\cdot}0\exp(-(0{\cdot}027)^2(V+32{\cdot}0)^2) + 4{\cdot}0$$

$$n_\infty = \frac{1{\cdot}0}{1+\exp([V-7{\cdot}18701]/-11{\cdot}77468)}$$

$I_{K,Ca}$: calcium-activated potassium current

$$I_{K,Ca} = \bar{g}_{K,Ca}\, c(V - E_K)$$

$$\dot{c} = \frac{c_\infty - c}{\tau_c}$$

$$\alpha_c = 75{\cdot}0[Ca^{2+}]_i \exp\left(\frac{V+20{\cdot}0}{24{\cdot}0}\right)$$

$$\beta_c = 0{\cdot}2\exp\left(\frac{V+20{\cdot}0}{-24{\cdot}0}\right)$$

$$\tau_c = \frac{0{\cdot}6}{\alpha_c+\beta_c}$$

$$c_\infty = \frac{\alpha_c}{\alpha_c+\beta_c}$$

Background currents

Inward rectifier current (I_R). Inward rectification has been observed in adult and neonatal rat ventral NTS neurons (vNTS) (Haddad & Getting, 1989). Functionally, I_R is similar to the I_q current found in hippocampal cells (Halliwell & Adams, 1982; Brown, Gähwiler, Griffith & Halliwell, 1990) in that it does not contribute to the normal action potential of the neuron, but serves to resist large

TABLE 3. Voltage- and concentration-dependent currents

I_R: inward rectifier current

$$I_R = \bar{g}_R \frac{(V - E_K - 36{\cdot}0)}{1 + \exp([(V - E_K + 140{\cdot}0)ZF]/RT)}$$

I_B: background current

$$I_B = I_{Na,B} + I_{K,B} = \bar{g}_{Na,B}(V - E_{Na}) + \bar{g}_{K,B}(V - E_K)$$

I_{NaCa}: sodium–calcium exchanger current

$$I_{NaCa} = K_{NaCa} \frac{DF_{in} - DF_{out}}{S}$$

$$S = 1 + D_{NaCa}([Ca^{2+}]_i [Na^+]_o^r + [Ca^{2+}]_o [Na^+]_i^r)$$

$$DF_{in} = [Na^+]_i^r [Ca^{2+}]_o \exp\left(\frac{(r-2)\gamma VF}{RT}\right)$$

$$DF_{out} = [Na^+]_o^r [Ca^{2+}]_i \exp\left(\frac{(r-2)(\gamma-1)VF}{RT}\right)$$

I_{CaP}: calcium pump current

$$I_{CaP} = \bar{I}_{CaP}\left(\frac{[Ca^{2+}]_i}{[Ca^{2+}]_i + K_{M,CaP}}\right)$$

I_{NaK}: sodium–potassium pump current

$$I_{NaK} = \bar{I}_{NaK}\left(\frac{[Na^+]_i}{[Na^+]_i + K_{M,Na}}\right)^3 \left(\frac{[K^+]_o}{[K^+]_o + K_{M,K}}\right)^2 \left(\frac{V + 150}{V + 200}\right)$$

hyperpolarizing deviations from the resting potential. We have treated I_R as a weak instantaneous, mixed-cation (Na^+ and K^+) current with a reversal potential of -44 mV. The mathematical description of this current (Table 3) was adapted from an analysis on the R15 neuron in *Aplysia* (Canavier, Clark & Byrne, 1991).

Background current (I_B). A linear background current I_B has also been included in our model as it is in most models of excitable cells (Yamada *et al.* 1989; Canavier *et al.* 1991; Belluzzi & Sacchi, 1991). However, there is no experimental data available in the published literature upon which to base functional descriptions of this current. This current is quite small and experiments to discern its ion transfer characteristics are essentially at the limit of practical resolution of whole-cell current recordings. We therefore assume that I_B represents the net sum of linear Na^+ ($I_{Na,B}$) and K^+ ($I_{K,B}$) background currents (Table 3), where the reversal potentials for these currents are E_{Na} and E_K, respectively.

Pump and exchanger currents

Virtually all excitable cells utilize ion exchanger mechanisms and ATP-dependent pumps in order to maintain intracellular chemical homeostasis. In our model, membrane potential is established through the net movement of Na^+, K^+ and Ca^{2+} ions. Therefore, only those mechanisms

known to participate in the active transport of these ions across the neural membrane were considered. Initial values for $[Na^+]_i$, $[K^+]_i$ and $[Ca^{2+}]_i$ were obtained from the literature (Schwarz & Eikhof, 1987), while the values for external concentrations matched those of the bathing medium in the brainstem slice preparation.

Sodium–calcium exchanger current (I_{NaCa})

The mathematical formulation for I_{NaCa} (Table 3) is comparable to that used by Rasmusson, Clark, Giles, Shibata & Campbell (1990) in describing Na^+–Ca^{2+} exchange associated with a cardiac myocyte (see Mullins (1981) for derivation and DiFrancesco & Noble (1985) for an explanation of the various parameters). The particular stoichiometry assumed for the exchanger in our model is 4:1, i.e. four Na^+ ions are exchanged for one Ca^{2+} ion, and is consistent with other neuronal models (Canavier *et al.* 1991). This ratio results in a net charge imbalance which produces a weakly depolarizing current over the majority of the action potential. Since $[Ca^{2+}]_o$, $[Na^+]_i$ and $[Na^+]_o$ have been held constant in this model, I_{NaCa} essentially reduces to a simplified form dependent only upon $[Ca^{2+}]_i$ and membrane voltage, V.

Calcium pump current (I_{CaP})

The calcium pump is a low-capacity, high-affinity electrogenic transport mechanism that increases with increasing $[Ca^{2+}]_i$. The Ca^{2+} efflux associated with this ATP-driven system is often referred to as 'uncoupled' to differentiate it from that associated with I_{NaCa} and is responsible for setting and maintaining very low resting levels of $[Ca^{2+}]_i$. The maximal pump current, $\bar{I}_{CaP}$, was assumed to be 10 pA with a Michaelis constant of $K_{M,CaP} = 0{\cdot}5\ \mu M$ (Caroni, Zurini, Clark & Carafoli, 1983) (Table 3).

Sodium–potassium pump current (I_{NaK})

The Na^+–K^+ pump is electrogenic and responsible for moving Na^+ and K^+ across the cell membrane, against their electrochemical gradient. The mathematical description of I_{NaK} (Table 3) is identical to that proposed by Rasmusson *et al.* (1990) where the concentration-dependent terms are exponentiated (2 for activation by $[K^+]_o$ and 3 for activation by $[Na^+]_i$) to reflect the well-known 3:2 stoichiometry of the Na^+–K^+ pump. Since the concentrations of Na^+ and K^+ in the intra- and extracellular media are assumed constant, I_{NaK} is essentially an instantaneous function of membrane voltage and responds proportionately with the action potential waveform.

Fluid compartment model

Our model takes into account the behaviour of Ca^{2+} both inside and outside the cell. The dynamics of $[Ca^{2+}]_i$ are of particular interest here since Ca^{2+} is known to influence the activation of $I_{K,Ca}$ and, in turn, affect SFA. Three processes that regulate $[Ca^{2+}]_i$ have been modelled: (a) entry, (b) buffering and (c) extrusion.

Calcium buffering. We have modelled the dynamic buffering of intracellular Ca^{2+} as binding to intracellular protein with the assumption that it is much more significant than Ca^{2+} binding by intracellular organelles. In the absence of precise knowledge of the type of cytosolic buffer in NTS neurons, we have assumed that the main buffer present is similar to the ubiquitous protein, calmodulin, with four separate Ca^{2+} binding sites (McBurney & Neering, 1987; Robertson, Johnson & Potter, 1981). The relatively large molecular weight of such proteins should allow negligible diffusion of buffer molecules over the time scale of interest. Ca^{2+} binding to the intracellular buffer has been treated as a first-order process described by the following differential equation for the temporal rate of change of occupancy of calcium binding sites (Robertson *et al.* 1981; Thayer & Miller, 1990):

$$\dot{O}_C = k_U[Ca^{2+}]_i(1-O_C) - k_R O_C, \tag{3}$$

where, O_C is the buffer occupancy, i.e. the fraction of sites already occupied by Ca^{2+}, and therefore unavailable for calcium binding; k_U and k_R are the first-order kinetic rate constants for Ca^{2+} uptake and release, respectively (see Table 4 for parameter values and units). Such calcium buffering reduces the amount of free $[Ca^{2+}]_i$. However, to maintain Ca^{2+} homeostasis, the remaining ions must ultimately be removed and this is accomplished by means of the two conventional transport systems, I_{NaCa} and I_{CaP}.

Material balance for calcium. The rate of change of free $[Ca^{2+}]_i$ is described by the differential equation:

$$[Ca^{2+}]_i = \frac{I_{NaCa} - I_{Ca,L} - I_{CaP}}{2v_{Ca}F} - n[B]_i \dot{O}_C, \quad (4)$$

where v_{Ca} is the effective cell volume (in nl), F is Faraday's constant, $[B]_i$ is the internal concentration of the cytosolic buffer (mM), and n is the number of binding sites for Ca^{2+} on the buffer molecule. The value for v_{Ca} was set equal to 0·002 nl reflecting the assumption that roughly 10% of the cell volume is occupied by organelles (e.g. mitochondria, endoplasmic reticulum etc.).

TABLE 4. Computational parameters

Model parameters

$\bar{g}_{Na} = 0{\cdot}500\ \mu S$	$E_{Na} = 75$ mV	$[Na^+]_o = 154$ mM
$\bar{g}_{Ca,L} = 0{\cdot}075\ \mu S$	$E_{Ca,L} = 50$ mV	$[Ca^{2+}]_o = 2{\cdot}4$ mM
$\bar{g}_K = 1{\cdot}100\ \mu S$	$E_K = -80$ mV	$[K^+]_o = 5{\cdot}9$ mM
$\bar{g}_A = 0{\cdot}205\ \mu S$	$\bar{g}_D = 0{\cdot}300\ \mu S$	$[Na^+]_i = 8{\cdot}71$ mM
$\bar{g}_{K,Ca} = 0{\cdot}185\ \mu S$	$\bar{g}_R = 0{\cdot}100\ \mu S$	$[K^+]_i = 155$ mM
$\bar{g}_{Na,B} = 0{\cdot}0009315\ \mu S$	$\bar{g}_{K,B} = 0{\cdot}0009935\ \mu S$	$F = 96500$ C mol^{-1}
$C_m = 0{\cdot}052$ nF	$v_{Ca} = 0{\cdot}002$ nl	$R = 8314$ J kg^{-1} mol^{-1} K^{-1}
$\bar{I}_{CaP} = 0{\cdot}01$ nA	$\bar{I}_{NaK} = 0{\cdot}15$ nA	$T = 310$ K
$D_{NaCa} = 0{\cdot}05$ mM^{-4}	$[B]_i = 0{\cdot}04$ mM	$K_{NaCa} = 0{\cdot}00016$ nA mM^{-4}
$K_{M,CaP} = 0{\cdot}0005$ mM	$K_{M,Na} = 5{\cdot}46$ mM	$K_{M,K} = 0{\cdot}621$ mM
$k_U = 100$ mM^{-1} ms^{-1}	$k_R = 0{\cdot}238$ ms^{-1}	$Z = 1{\cdot}0$
$\gamma = 0{\cdot}5$	$r = 4$	$n = 4$

State variable initial conditions

$V = -42{\cdot}116310$ mV $\quad [Ca^{2+}]_i = 0{\cdot}000049$ mM

$m = 0{\cdot}041904$	$h = 0{\cdot}923234$	$n = 0{\cdot}015467$
$d_L = 0{\cdot}018110$	$f_L = 0{\cdot}998023$	$p = 0{\cdot}666418$
$q_1 = 0{\cdot}004915$	$q_2 = 0{\cdot}008894$	$x = 0{\cdot}311018$
$y = 0{\cdot}056171$	$c = 0{\cdot}002932$	$O_C = 0{\cdot}020856$

Computational aspects

We have modelled the soma of the mNTS neuron as a prolate spheroid with a major and minor axis of 51 and 9 μm, respectively, based on measurements of Lucifer Yellow-filled mNTS cells (M. Andresen & M. Yang, unpublished results). The whole-cell membrane capacitance, C_m, was set to 52 pF. The model consists of thirteen coupled, first-order, non-linear differential equations; eleven associated with the ion fluxes across the cell membrane, and two describing the fluid compartments. A fifth-order Runge–Kutta–Merson numerical integration algorithm (Novikov & Novikov, 1987), which varies its temporal step size in accordance with an estimate of the integration error, was used to solve this relatively stiff system of non-linear equations. To ensure accuracy, local error estimates on all state variables were maintained below 10^{-8} and double precision was selected in all computations. The programs were written in the 'C' programming language, and the computations were performed on a Sun Microsystems Sparc II workstation.

The nominal parameter values and state variable initial conditions used in this modelling effort are presented in Table 4. Here, we present comprehensive model predictions for a single, complete set of model parameters and compare these to experimental data from a single representative mNTS neuron.

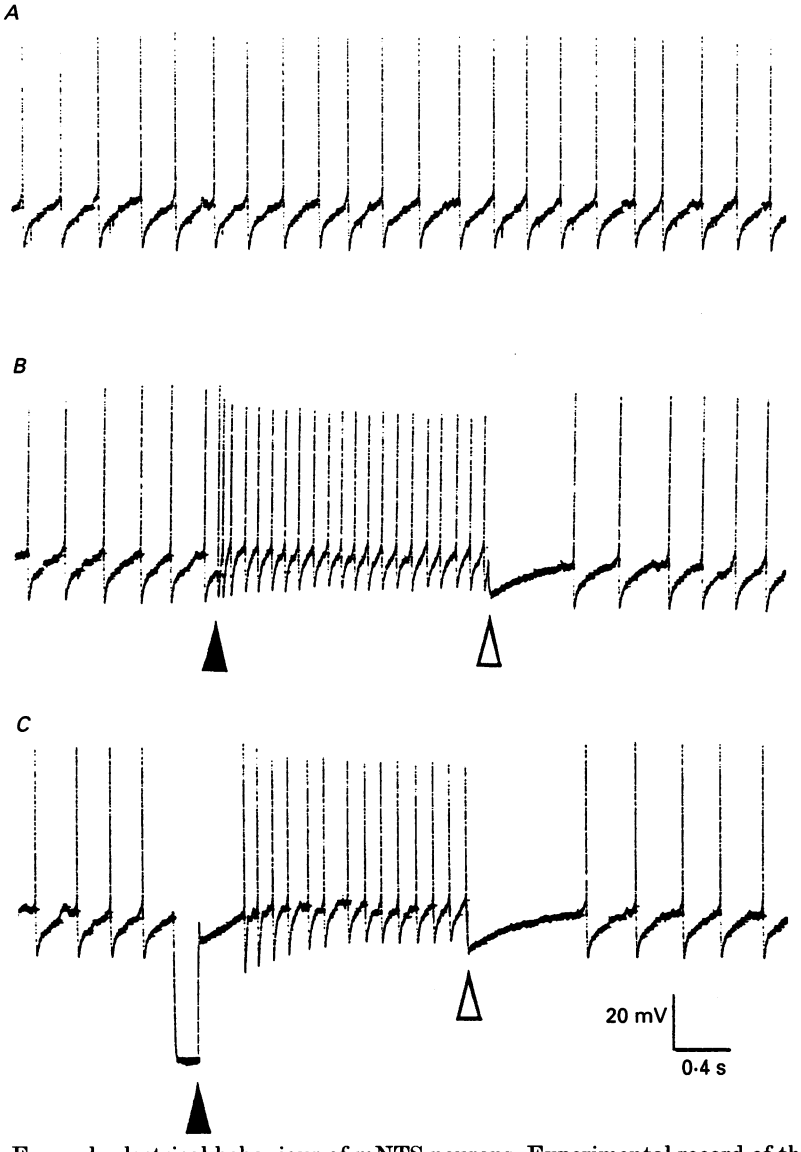

Fig. 3. Example electrical behaviour of mNTS neurons. Experimental record of the free-running 'beating' state of the mNTS neuron (trace *A*). Depolarization with current pulse of 0·15 nA for 2·0 s (trace *B*) transiently increased spike discharge rate in a manner consistent with spike frequency adaptation (SFA). The cell quickly recovered to its free-running state upon cessation of the depolarizing pulse. Preconditioning with a 200 ms hyperpolarizing current pulse (trace *C*) induced a prolonged delay in onset of firing even in the presence of a 0·15 nA depolarization current which was applied immediately upon termination of the preconditioning pulse. For all traces a filled arrowhead indicates start of the depolarizing stimulus while an open arrowhead indicates termination of this stimulus and return to rest conditions.

RESULTS

Electrical behaviour of mNTS neurons

All neurons studied in the brainstem slice preparation were found to be spontaneously active with firing frequencies in the range of 1–10 Hz (Fig. 3*A*). None exhibited bursting activity. Upon step depolarization from their baseline (−65 to −45 mV), these cells fired transiently at a rate several times greater than spontaneous activity. Spike frequency then declined rapidly, settling at a lower steady-state level (Fig. 3*B*) in a manner consistent with the phenomena of SFA. When the neurons were preconditioned with hyperpolarizing current pulses, the pattern of activity changed remarkably. DE was evident while SFA was essentially non-existent. Even in the presence of strong depolarizing current injections, the onset of firing was delayed by as much as hundreds of milliseconds (Fig. 3*C*). The hyperpolarizing prepulses also slightly decreased the firing rate during subsequent depolarization (compare Fig. 3*B* and *C*). All cells recorded exhibited both DE and SFA.

Spontaneous activity

A comparison of experimentally obtained and model-generated action potential data is shown in Fig. 4*A* for the case of free-running spontaneous activity. Note that membrane repolarization has two 'phases', with markedly different slopes. A steeper recovery occurs immediately after the action potential and is followed by a more gradual increase in membrane potential, up to the firing threshold. The derivative of membrane potential (dV/dt) throughout the interspike interval (ISI) was one of several measures utilized in identifying a complete model parameter set which provided the smallest error in the least-squares fit to our data. In this fitting process the background conductance parameters ($g_{Na,B}$ and $g_{K,B}$) were adjusted (symmetrically) to match this cell's average rest pacing rate of 4·3 Hz. The model also accurately reproduces the neuron's unique pattern of after-hyperpolarization (AHP) existent throughout the entire ISI (Fig. 4*B* and *C*).

Current pulse protocols

One of the major contributions of this mNTS modelling effort is that it suggests functional roles for the underlying membrane currents responsible for the unique patterns of electrophysiological activity observed in this cell. As with the experimental protocols, this striking diversity has been illustrated using a defined series of current pulse protocols intended to evoke the more remarkable patterns of neural activity recorded experimentally. In our simulations the injected current (I_{STIM}) was varied in accordance with the experimental protocol. Pulse width was maintained equivalent to that used in the experiments while amplitude was set to one-half the value used experimentally. Using a consistently lower value for I_{STIM} in the simulations is considered reasonable when the practical aspects of the experimental preparation are taken into account. For example, 'space-clamp' conditions are only achieved approximately in the brainstem slice preparation due to the presence of 'leakage pathways' as well as the potential for current flow through the neuron's dendritic structure. Therefore, not all of the current injected via the

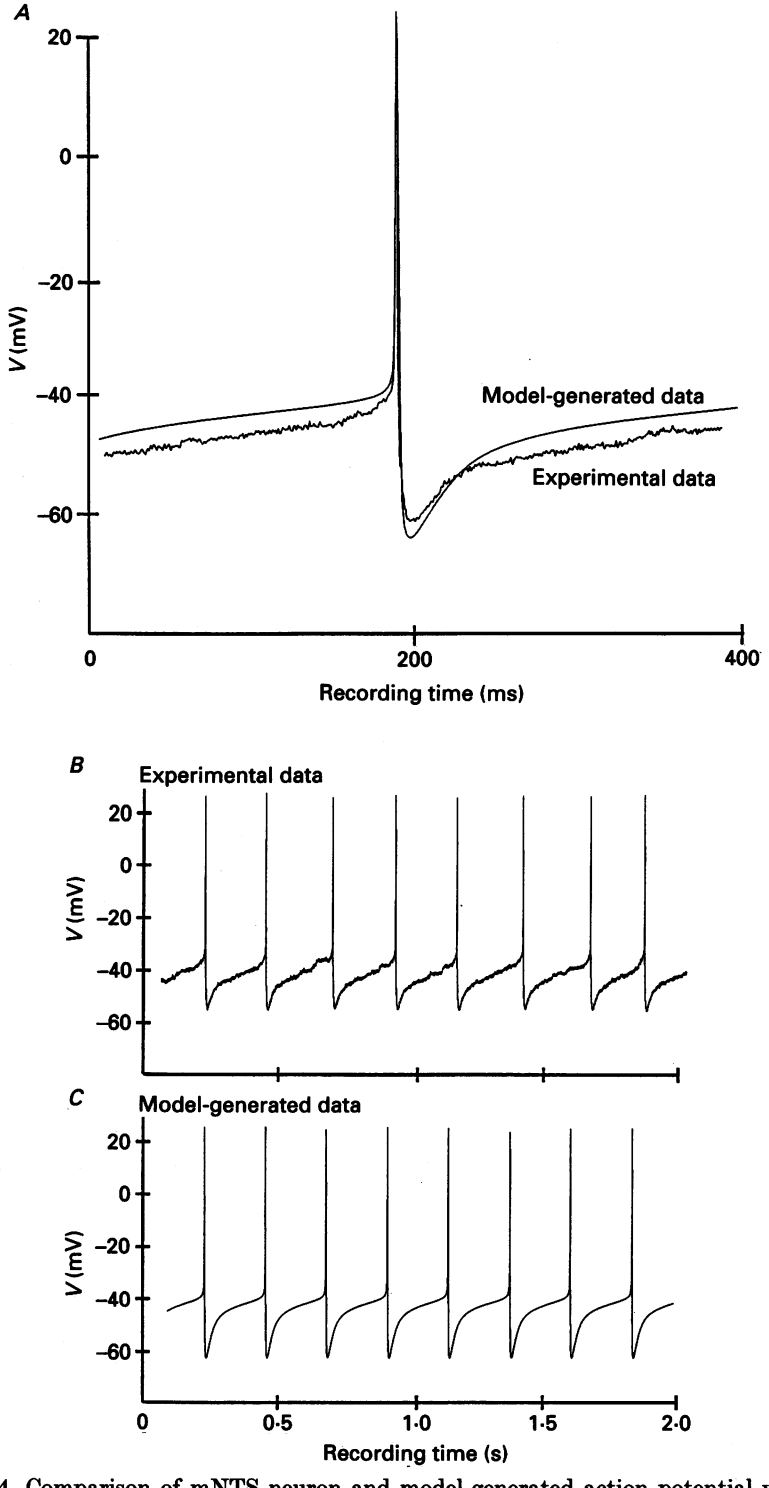

Fig. 4. Comparison of mNTS neuron and model-generated action potential waveforms recorded during normal pacing activity (Fig. 4*A*). The model is capable of reproducing the neuron's unique pattern of AHP existent throughout the entire interspike interval (ISI).

bridge circuit travels in a radial direction through the somatic membrane to depolarize the cell. The model assumes ideal space-clamp conditions and thus with no leakage, less current is required for depolarization. We have arbitrarily chosen a value of 50% for the leakage current.

Currents associated with spike frequency adaptation

The extent and time course of SFA in the experimental (discrete points, Fig. 5) and model-generated data (contiguous traces, Fig. 5) are quite comparable. This can best be illustrated by plotting instantaneous firing frequency (IFF) as a function of time. Upon depolarization from resting levels, both the neuron and the model exhibit an initial peak IFF which adapts quickly to a steady-state level. Preconditioning the cell and neuron model with a 200 ms hyperpolarization to −80 mV very strongly decreases the amount of SFA.

Direct comparison of SFA in experimental and model-generated records illustrates the great degree of consistency between the electrical behaviour of the mNTS cell and neuron model (Fig. 6*A* and *B*). Both records initially exhibit high-frequency activity upon stimulus application, which adapts to a lower maintained firing rate within approximately 500 ms. The dynamic response of the calcium-activated K^+ current ($I_{K,Ca}$) and intracellular calcium ($[Ca^{2+}]_i$) transient can also be predicted by the mNTS neuron model (Fig. 6, traces *C* and *D*, respectively). The initial increase in firing rate, following application of the depolarizing stimulus, results in an increase in $[Ca^{2+}]_i$. As $I_{K,Ca}$ is functionally dependent upon $[Ca^{2+}]_i$, it also begins to increase. This added outward current acts to reduce the neuron's net transmembrane current which results in a relatively slow decay to a sustained firing rate as $[Ca^{2+}]_i$ and $I_{K,Ca}$ reach new equilibrium values. Note also from Fig. 6*A* and *B* that there is a decrease in the magnitude of the slope of the secondary component of the pacemaker potential. This effect is quite noticeable during SFA and is caused by the increase in $I_{K,Ca}$ following application of the stimulus. In addition, the model is capable of reproducing the observed trend in the peak value of AHP associated with the action potentials of the response train.

Currents underlying delayed excitation

Comparison of membrane response in experimental and model-generated records under stimulus conditions necessary to evoke DE demonstrates the model's ability to reproduce this phenomenon accurately (Fig. 7*A* and *B*). The model predicts that the intrinsic pattern of delay observed between the onset of depolarization and the occurrence of the first action potential results primarily from the interaction between the internally applied stimulus current I_{STIM}, the intrinsic background current I_B and the transient outward K^+ currents I_A and I_D. I_A contributes a fast, outward current (Fig. 7*C*) which inhibits the cell from initially firing upon

In Fig. 4*A* the baseline of the action potential from this representative neuron has been shifted downward so as to more accurately reflect the average ($n = 10$) peak AHP potential of $-61{\cdot}32 \pm 4{\cdot}85$ mV (mean ± S.E.M.). The model is also capable of providing accurate fits to this neuron's basal firing rate (traces *B* and *C*). All experimental data have been filtered using an 11th order digital Butterworth design with a cut-off frequency of 2·0 kHz.

application of the depolarizing stimulus (see magnified insets, Fig. 7). We also find that the relatively slow second-order inactivation characteristics of I_A (see Table 2) are responsible for the bulk of DE. I_D, like I_A, exhibits rapid-activation characteristics but extremely slow inactivation. In fact, the 200 ms conditioning

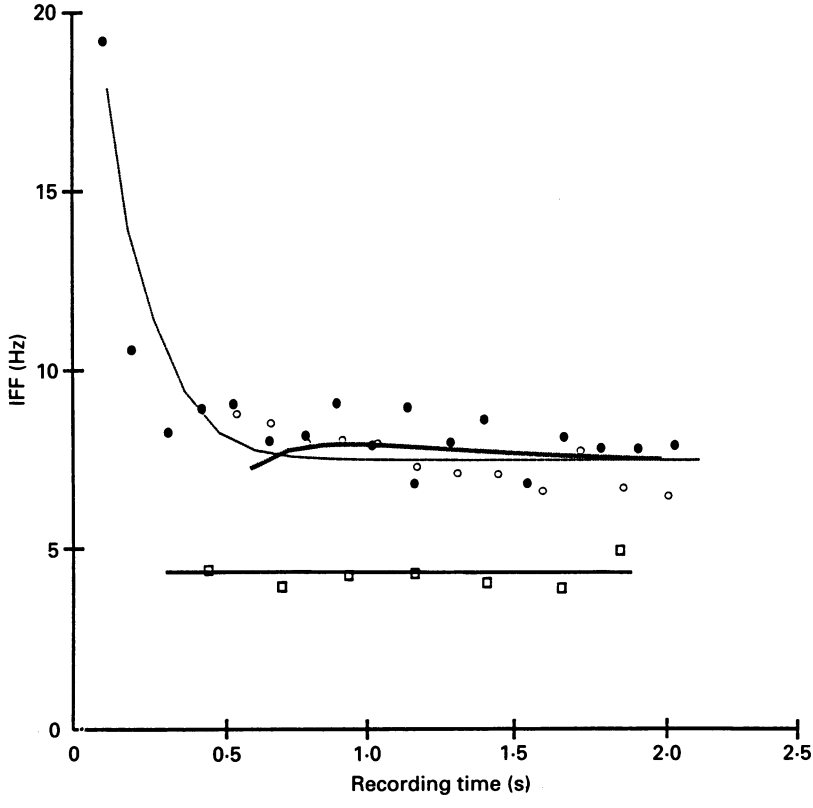

Fig. 5. Instantaneous firing frequency (IFF) as a function of recording time. At rest levels the model (continuous line) was tuned to match the average IFF of the mNTS neuron (□). With application of a 0·3 nA current stimulus both the mNTS neuron (●) and the model (thin dotted line) exhibit a transient rise in their IFF, a response which is characteristic of spike frequency adaptation (SFA). Preconditioning the neuron to a level of −80 mV for 200 ms prior to application of the 0·3 nA depolarizing stimulus virtually eliminated SFA in both the experimental (○) and model-generated (thick dotted line) records. For all measurements the experimental preparation and the computer simulation utilized the same stimulus current protocol.

prepulse is too short to evoke a significant change from steady-state values brought about by activation of this outward current (see Table 2). As a consequence, I_D contributes only a minor portion of the total outward current during DE (Fig. 7*D*). The net membrane current during the DE phase is inward, thus accounting for the gradual membrane depolarization up to the level of threshold for I_{Na}, where an action potential is produced. Following DE, I_A decays away in accordance with its second-order inactivation characteristics (τ_{q_1} = 70 ms and τ_{q_2} = 550 ms) to very low levels. I_D, however, remains as a significant outward background current. Due to its long time constant of inactivation (τ_D = 6500 ms), I_D functions much like an integrator,

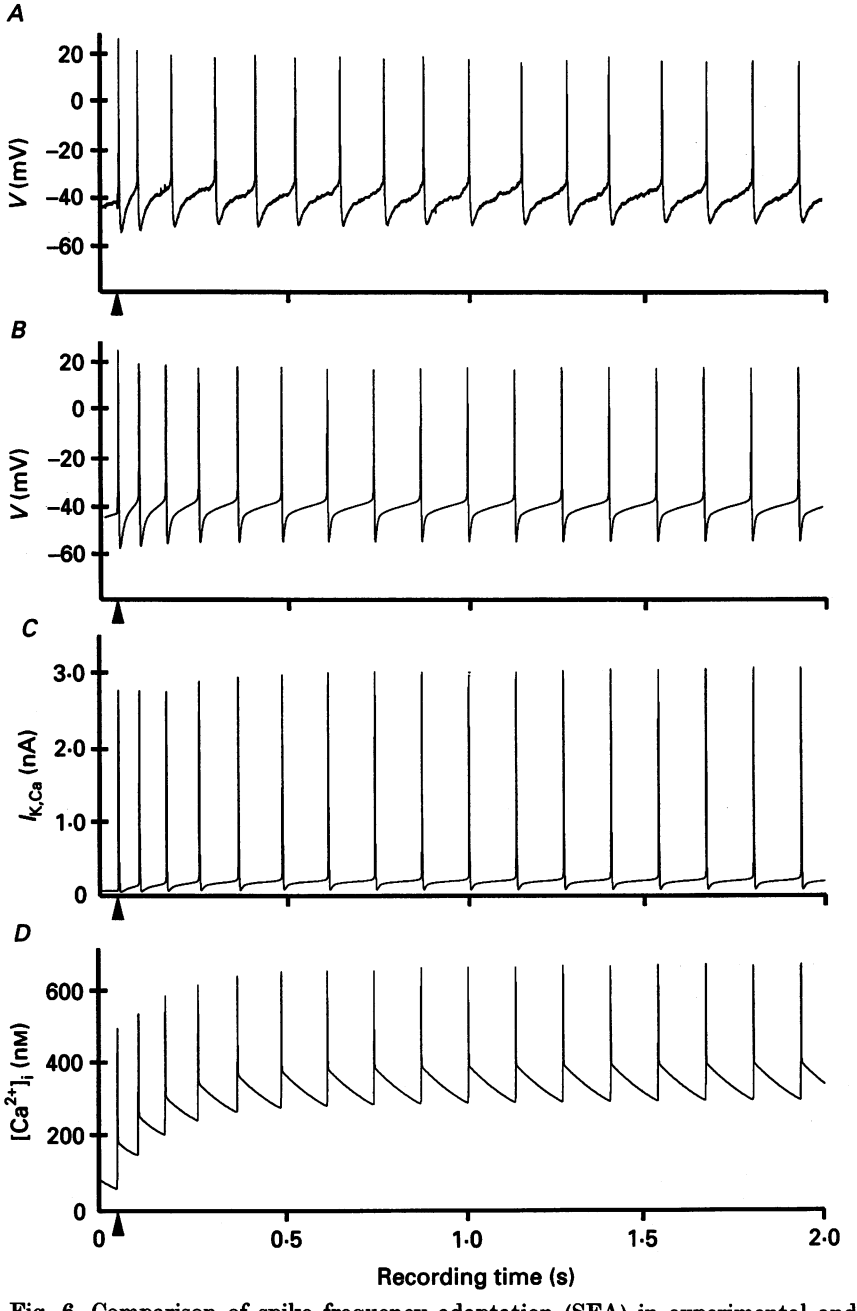

Fig. 6. Comparison of spike frequency adaptation (SFA) in experimental and model-generated records. Traces *A* and *B* illustrate the behaviour of the mNTS cell and neuron model, respectively, upon injection of a depolarizing current of 0·3 nA during rest activity. Both voltage records exhibit high-frequency activity upon application of the stimulus, which adapts to a lower steady-state firing rate after approximately 500 ms. Traces *C* and *D* demonstrate the dynamic response of $I_{K,Ca}$ and $[Ca^{2+}]_i$, respectively, as predicted by the mNTS neuron model. The initial increase in firing rate, concomitant with the depolarizing stimulus, results in a rise in $[Ca^{2+}]_i$ levels. As $I_{K,Ca}$ (trace *C*) is functionally dependent upon $[Ca^{2+}]_i$ (trace *D*), it also begins to increase. This added outward current acts to reduce the neuron's net transmembrane current which results in a relatively slow decay to a sustained firing rate as $[Ca^{2+}]_i$ and $I_{K,Ca}$ reach steady-state values. Arrowheads on abscissa indicate the application of a 0·3 nA depolarizing stimulus (I_{STIM}) from rest conditions which lasts the entire trace. The experimental data have been filtered using an 11th order digital Butterworth design with a cut-off frequency of 2·0 kHz.

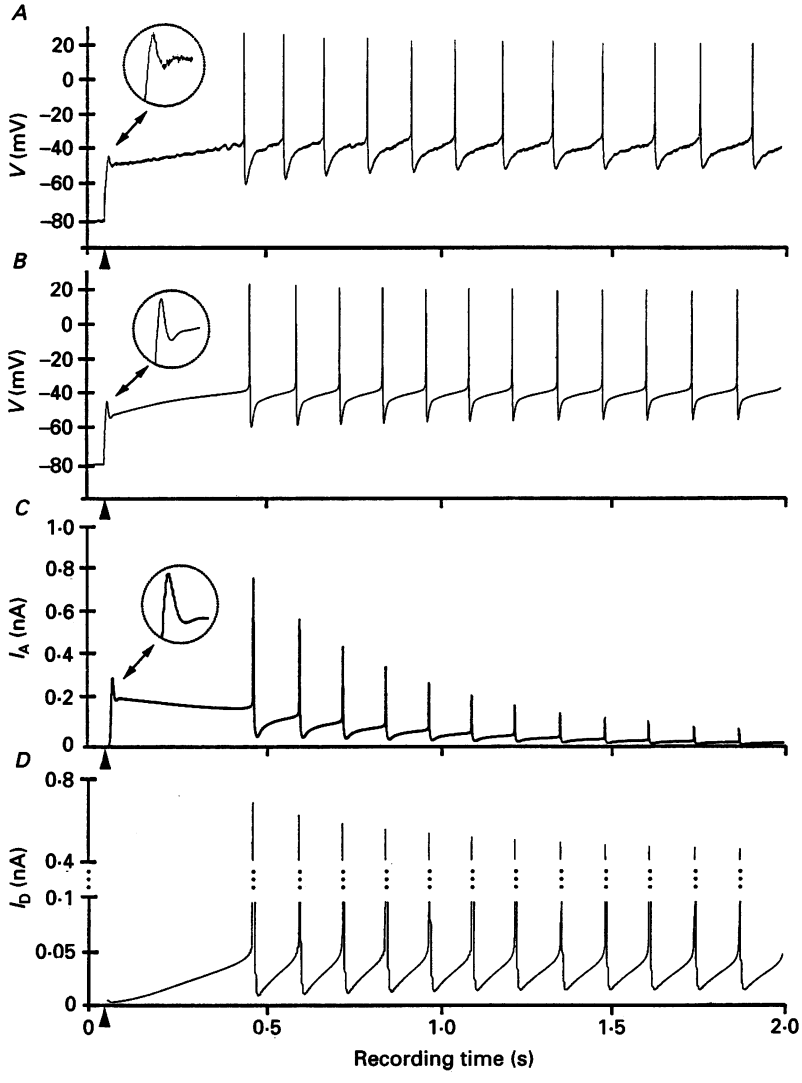

Fig. 7. Comparison of delayed excitation (DE) in experimental and model-generated records. Traces *A* and *B* illustrate the behaviour of the NTS cell and neuron model, respectively, upon injection of a 0·3 nA depolarizing current immediately after preconditioning to −80 mV for 200 ms using a −0·3 nA hyperpolarizing current pulse. Only the final 50 ms of the 200 ms hyperpolarization is shown and at 50 ms, the depolarizing current injection begins. The observed delay of approximately 400 ms is a result of the interaction between the depolarizing drive, the relatively weak background current I_B and the two transient outward K^+ currents, I_A (trace *C*) and I_D (trace *D*). Magnified insets demonstrate the rapid activation kinetics of I_A and the extent to which this current can suppress spike initiation. Arrowheads on abscissa demarcate transition of I_{STIM} from a 200 ms, −0·3 nA conditioning prepulse to a 0·3 nA depolarizing stimulus which lasts the entire trace. The experimental data have been filtered using an 11th order digital Butterworth design with a cut-off frequency of 2·0 kHz.

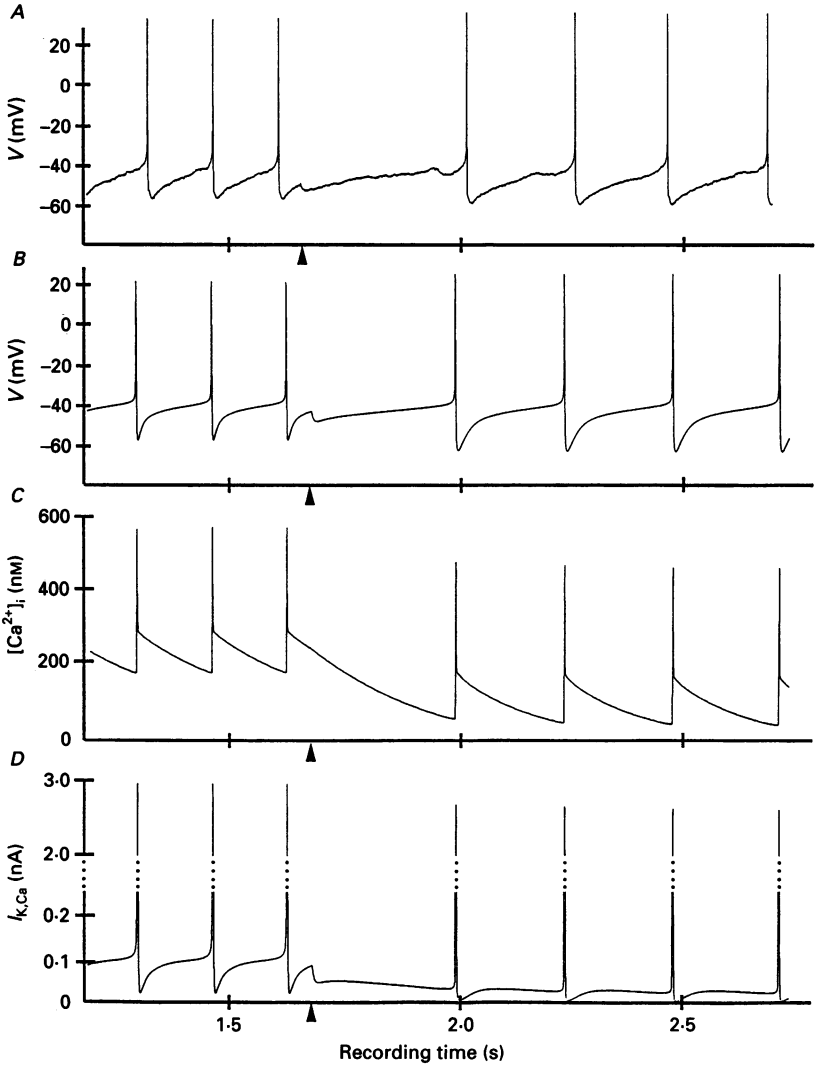

Fig. 8. Comparison of post-stimulus recovery characteristics in experimental and model-generated records. Traces *A* and *B* illustrate the behaviour of the membrane potential for the mNTS cell and neuron model, respectively, upon termination of a 0·15 nA depolarizing current. Traces *C* and *D* demonstrate the dynamic response of $[Ca^{2+}]_i$ and $I_{K,Ca}$, respectively, as predicted by the mNTS neuron model. With the removal of the external stimulus the rather strong net outward current dominated by $I_{K,Ca}$ causes membrane voltage to hyperpolarize. As $[Ca^{2+}]_i$ levels decay so follows total $I_{K,Ca}$. Arrowheads on abscissa demarcate the transition of I_{STIM} from a 0·15 nA depolarizing stimulus to 0·0 nA which continues for the remainder of the trace. The experimental data have been filtered using an 11th order digital Butterworth design with a cut-off frequency of 2·0 kHz.

slowly raising its average current contribution as firing rate increases. If this higher rate is sustained, the net increase in total outward current (I_D as well as $I_{K,Ca}$) inhibits further increases in firing rate.

It is also interesting to note that the positive peak potential and peak AHP of the first action potential following the DE phase, are slightly greater than those in the

steady state (compare first and last action potentials of the experimental and model-generated records in Fig. 7, traces *A* and *B*, respectively). The model predicts this subtle 'fade-away' in the peak-to-peak magnitude of the action potential waveform and suggests that the response characteristics of I_A, I_D and $I_{K,Ca}$ contribute to this pattern of activity. This effect is even more pronounced in the absence of the preconditioning hyperpolarization (compare Fig. 6*A* and *B* with Fig. 7*A* and *B*). Thus, $I_{K,Ca}$ plays an important role in SFA, I_A is instrumental in producing DE and both I_D and $I_{K,Ca}$ are quite important in determining the neuron's maintained steady-state firing rate.

Post-stimulation recovery

The model is also capable of reproducing the passive electrophysiological characteristics of the mNTS neuron following cessation of a depolarizing current. Simulations demonstrate that restoration of baseline membrane potential after cessation of a depolarizing pulse is quite consistent with experimental observations (Fig. 8*A* and *B*). The depolarizing stimulus causes a general elevation in the average level of $[Ca^{2+}]_i$ and upon termination of the pulse (note arrowheads in Fig. 8), the level of $[Ca^{2+}]_i$ gradually decays (Fig. 8*C*). The duration and character of this 'recovery' phase is determined by the amount of $[Ca^{2+}]_i$ that has accumulated during the course of accelerated spiking, and its subsequent removal by the Ca^{2+} pump and Na^+–Ca^{2+} exchanger. The rather strong net outward current contributed primarily by $I_{K,Ca}$, I_D and I_K, forces membrane voltage to hyperpolarize following loss of the external stimulus. As $[Ca^{2+}]_i$ levels decay so follows total $I_{K,Ca}$. Once resting levels of $[Ca^{2+}]_i$ have been restored, spiking resumes at its basal rate. This decrease in $[Ca^{2+}]_i$ following termination of the pulse necessarily results in a weaker expression of $I_{K,Ca}$ during post-stimulus firing (note peak height of $I_{K,Ca}$ in Fig. 8*D*).

DISCUSSION

A longitudinal brainstem slice preparation from adult rats was used to study the responses of mNTS neurons to hyperpolarizing and depolarizing current pulses. To further understand the ionic mechanisms underlying the electrical behaviour of these cells, we developed a generic HH-type ion channel model based, in part, upon whole-cell voltage-clamp recordings from our laboratory of enzymatically dispersed mNTS neurons in guinea-pig. The model provides reasonably accurate fits to action potential waveforms recorded from the brainstem slice preparation (Fig. 4*A*, *B* and *C*). More exact reproduction of this neuron's action potential than presently afforded by our model would require a thorough characterization of $[Ca^{2+}]_i$ dynamics as well as the delicate balance of exchanger and pump currents. To date, such data from mNTS neurons is not available. However, the model in its present form is capable of mimicking the more outstanding patterns of electrical activity in mNTS neurons. Direct comparison of model-generated and experimentally recorded data has been presented for a variety of phenomena such as spike frequency adaptation (SFA) (see Figs 5 and 6) and delayed excitation (DE) (see Fig. 7), which are commonly exhibited by many types of NTS neurons in different species (Champagnat *et al.* 1986; Dekin & Getting, 1987; Dekin, Getting & Johnson, 1987; Dekin & Haddad, 1990; Bradley & Sweazy, 1992).

The present data on delayed excitation are very similar to those reported for one class of neurons in the guinea-pig vNTS (Dekin *et al.* 1987). Type II neurons were reported to be generally fusiform in shape and exhibited substantial DE upon hyperpolarization. Half-maximal delays for these type II vNTS neurons occurred with prepulses to about −75 mV and prepulse durations of about 50–100 ms. A similar pattern of DE has been reported for one of several characterized cell types in the rostral gustatory zone of rat NTS (Bradley & Sweazy, 1992). Our results in rat mNTS neurons receiving synaptic input from the solitary tract appear morphologically and electrophysiologically quite similar to these type II guinea-pig ventral neurons. By comparison, however, we have found no evidence for neurons comparable to the guinea-pig type I neurons which had very rapid and complete SFA patterns. In our studies of rat mNTS, patterns of DE are markedly similar across neurons which both are and *are not* connected to the tract but which have a stellate appearance (M. Andresen & M. Yang, unpublished observations). These neurons resemble the guinea-pig type III morphology (Dekin *et al.* 1987). Type III guinea-pig vNTS neurons, however, had no SFA.

Potential of delayed excitation

Measurements of the delay between baroreceptor stimulation and the baroreflex responses in the cat, yield values that fall into two ranges (20–60 and 70–110 ms) suggesting the involvement of two pathways (McAllen & Spyer, 1978). If the shortest pathway in this reflex involves only two central neurons, a mNTS projection neuron and a preganglionic parasympathetic motoneuron located in the nucleus ambiguus, then, clearly, even the smallest central delay in the reflex (20 ms) is relatively long for such a simple polysynaptic pathway. Our *in vitro* studies on the rat brainstem slice preparation and model simulations show that under appropriate conditions (e.g. pre-hyperpolarization), mNTS neurons can exhibit delays over a wide range (hundreds of milliseconds). Thus, if our results are indicative of mNTS neurons receiving baroreceptor inputs, longer central delays *in vivo* may involve the DE mechanism. Inhibitory inputs to mNTS neurons would be required to provide an adequate hyperpolarization for a sufficient period of time. Such inhibitory inputs to mNTS neurons could provide the substrate necessary to express DE, by facilitating the expression of I_A and I_D through membrane hyperpolarization. *In vivo* intracellular studies (Mifflin & Felder, 1990) show that the electrical stimulation of projections from higher centres such as the nucleus parabrachialis and hypothalamic defence area can evoke strong inhibitory responses in NTS neurons.

Model applicability

Reported observations on slice preparations of NTS neurons indicate considerable heterogeneity within and across species. For instance, two types of vNTS neurons have been described in the rat (Haddad & Getting, 1989) and three subtypes have been reported in the guinea-pig (Dekin & Getting, 1987; Dekin *et al.* 1987). By comparison, rat mNTS neurons receiving solitary tract afferent input are remarkably homogeneous in their electrophysiological properties. Nevertheless, the full complement of ionic current types present in the guinea-pig vNTS cells appears to be present in the ventral and medial NTS neurons of the rat. Thus, although these classifications are not preserved across species, the fundamental repertoire of cellular

firing properties characterizing these neurons remains consistent. It is highly probable that all neurons in the NTS possess nearly the same molecular species of ion channels, but it is their relative expression that affords differences in electrical behaviour.

As a working hypothesis, this model formulation shows remarkable promise in its general predictive capacity and as a testing medium. For its relative simplicity, the model mimics both changes in action potential form, the time course of membrane potential during the intraspike interval and the exacting membrane potential trajectories of spike frequency adaptation, delayed excitation and post-stimulus recovery. Modification of model parameters could reflect differential expression of ion channels across neuron types. As such experimental data become available, model parameters can be adjusted in order to simulate the electrical behaviour of the various NTS cells described to date.

The authors would like to acknowledge the generous financial support of the Biomedical Engineering Center, University of Texas Medical Branch, Galveston, TX. This project was also supported in part by NSF CISE-II grant CCR8619893 and in part by grants awarded to M.C.A. from National Institutes of Health (HL-41119) and American Heart Association (91-6780).

REFERENCES

ANDRESEN, M. & YANG, M. (1990). Non-NMDA receptors mediate sensory afferent synaptic transmission in medial nucleus tractus solitarius. *American Journal of Physiology* **259**, H1307–1311.

BELLUZZI, O. & SACCHI, O. (1989). Calcium currents in the normal adult rat sympathetic neurone. *Journal of Physiology* **412**, 493–512.

BELLUZZI, O. & SACCHI, O. (1991). A five-conductance model of the action potential in the rat sympathetic neurone. *Progress in Biophysics and Molecular Biology* **55**, 1–30.

BRADLEY, R. & SWEAZY, R. (1992). Separation of neuron types in the gustatory zone of the nucleus tractus solitarii on the basis of intrinsic firing properties. *Journal of Neurophysiology* **67**, 1659–1668.

BROWN, D., GÄHWILER, B., GRIFFITH, W. & HALLIWELL, J. (1990). Membrane currents in hippocampal neurones. *Progress in Brain Research* **83**, 141–160.

CANAVIER, C., CLARK, J. & BYRNE, J. (1991). Simulation of the bursting activity of neurone R15 in *Aplysia*: role of ionic currents, calcium balance and modulatory transmitters. *Journal of Neurophysiology* **66**, 2107–2124.

CARONI, P., ZURINI, M., CLARK, A. & CARAFOLI, E. (1983). Further characterization and reconstitution of the purified Ca-pumping ATPase of the heart sarcolemma. *Journal of Biological Chemistry* **258**, 7305–7310.

CHAMPAGNAT, J., JACQUIN, T. & RICHTER, D. (1986). Voltage-dependent currents in neurones of the nuclei of the solitary tract of rat brainstem slices. *Pflügers Archiv* **406**, 372–379.

CIRIELLO, J. (1983). Brainstem projections of aortic baroreceptor afferent fibres in the rat. *Neuroscience Letters* **36**, 37–42.

DEKIN, M. & GETTING, P. (1987). In vitro characterization of neurones in the ventral part of the nucleus tractus solitarius. II. Ionic basis for repetitive firing patterns. *Journal of Neurophysiology* **58**, 215–229.

DEKIN, M., GETTING, P. & JOHNSON, S. (1987). In vitro characterization of neurones in the ventral part of the nucleus tractus solitarius. I. Identification of neuronal types and repetitive firing properties. *Journal of Neurophysiology* **58**, 195–214.

DEKIN, M. & HADDAD, G. (1990). Membrane and cellular properties in oscillating networks: implications for respiration. *Journal of Applied Physiology* **69**, 809–821.

DIFRANCESCO, D. & NOBLE, D. (1985). A model of cardiac electrical activity, ionic pumps, and concentration changes. *Philosophical Transactions of the Royal Society* B **222**, 353–398.

GREENE, R., HAAS, H. & REINER, P. (1990). Two transient outward currents in histamine neurones of the rat hypothalamus *in vitro*. *Journal of Physiology* **420**, 149–163.

HADDAD, G. & GETTING, P. (1989). Repetitive firing properties of neurones in the ventral region of nucleus tractus solitarius. In vitro studies in adult and neonatal rat. *Journal of Neurophysiology* **2**, 1213–1224.

HALLIWELL, J. & ADAMS, P. (1982). Voltage-clamp analysis of muscarinic excitation in hippocampal cells. *Brain Research* **250**, 71–92.

HODGKIN, A. & HUXLEY, A. (1952). A quantitative description of membrane current and its application to conduction and excitation in nerve. *Journal of Physiology* **117**, 500–544.

KASAI, H., KAMEYAMA, M., YAMAGUCHI, K. & FUKUDA, J. (1986). Single transient K channels in mammalian sensory neurones. *Biophysical Journal* **49**, 1243–1247.

KUNZE, D. (1987). Calcium currents of cardiovascular neurones isolated from adult guinea pigs. *American Journal of Physiology* **252**, H867–871.

KUNZE, D., YANG, M. & ANDRESEN, M. (1990). Identification of individual neurones receiving baroreceptor afferent innervation. *FASEB Journal* **4**, A1192 (abstract).

LOEWY, A. (1990). Central autonomic pathways. In *Central Regulation of Autonomic Functions*, ed. LOEWY, A. & SPYER, K., pp. 88–103. Oxford University Press, NY, USA.

MCALLEN, R. & SPYER, K. (1978). The baroreceptor input to cardiac vagal motoneurones. *Journal of Physiology* **282**, 365–374.

MCBURNEY, R. & NEERING, I. (1987). Neuronal calcium homeostasis. *Trends in Neurosciences* **10**, 164–169.

MARQUARDT, D. (1963). An algorithm for least-squares estimation of nonlinear parameters. *Journal of the Society for Industrial and Applied Mathematics* **11**, 431–441.

MENDELOWITZ, D., YANG, M., ANDRESEN, M. & KUNZE, D. (1992). Localization and retention in-vitro of fluorescently labeled aortic baroreceptor terminals on neurons from the nucleus tractus solitarius. *Brain Research* **581**, 339–343.

MIFFLIN, S. & FELDER, R. (19[illegible]). Synaptic mechanisms regulating cardiovascular afferent inputs to solitary tract nucleus. *American Journal of Physiology* **259**, H653–661.

MULLINS, L. (1981). *Ion Transport in Heart*. Raven, New York.

NOVIKOV, V. & NOVIKOV, E. (1987). Explicit methods for stiff systems of ordinary differential equations. In *Computational Mathematics II: Proceedings of the Second International Conference on Numerical Analysis and its Applications*, ed. FATUNLA, S., pp. 162–174. Boole, Dublin, Ireland.

NUMANN, R., WADMAN, W. & WONG, R. (1987). Outward currents of single hippocampal cells from adult guinea-pig. *Journal of Physiology* **393**, 331–353.

RASMUSSON, R., CLARK, J., GILES, W., SHIBATA, E. & CAMPBELL, D. (1990). A mathematical model of a bullfrog cardiac pacemaker cell. *American Journal of Physiology* **259**, H352–369.

REIS, D. (1984). The brain and hypertension: reflections on 35 years of inquiry into the neurobiology of the circulation. *Circulation* **70**, sIII, 31–45.

ROBERTSON, S., JOHNSON, J. & POTTER, J. (1981). The time course of Ca^{2+} exchange with calmodulin, troponin, and myosin in response to transient increases in Ca^{2+}. *Biophysical Journal* **34**, 559–569.

ROGAWSKI, M. (1985). The A-current: how ubiquitous a feature of excitable cells is it? *Trends in Neurosciences* **8**, 214–219.

SAPRU, H. & KRIEGER, A. (1977). Carotid and aortic chemoreceptor function in the rat. *Journal of Applied Physiology* **42**, 344–348.

SCHWARZ, J. & EIKHOF, G. (1987). Na currents and action potentials in rat myelinated nerve fibres at 20 and 37 °C. *Pflügers Archiv* **409**, 569–577.

STORM, J. (1988). Temporal integration by a slowly inactivating K^+ current in hippocampal neurones. *Nature* **336**, 379–381.

THAYER, S. & MILLER, R. (1990). Regulation of the intracellular free calcium concentration in single rat dorsal root ganglion neurones *in vitro*. *Journal of Physiology* **425**, 85–115.

THORN, W., WANG, X. & LEMOS, J. (1991). A fast, transient K^+ current in neurohypophysial nerve terminals of the rat. *Journal of Physiology* **432**, 313–326.

YAMADA, W., KOCH, C. & ADAMS, P. (1989). Multiple channels and calcium dynamics. In *Methods in Neuronal Modeling: From Synapses to Networks*, ed. KOCH, C. & SEGEV, I., pp. 97–133. MIT Press, Cambridge, MA, USA.

ZBCIZ, K. & WEIGHT, F. (1985). Transient voltage and calcium-dependent outward currents in hippocampal CA3 pyramidal neurones. *Journal of Neurophysiology* **53**, 1038–1058.